Light-Induced Intramolecular Electron Transfer in a 1D [CuFe] Coordination Polymer Containing the $[Fe(C_2O_4)_3]^{3-}$ Core

Lidija Molčanov,[a] Lidija Androš Dubraja,[a] Dijana Žilić,[a] Krešimir Molčanov,[a]

*Dario Barišić,[b] Damir Pajić,[b] Ivor Lončarić,[a] Ana Šantić[a] and Marijana Jurić[a,]**

[a]Ruđer Bošković Institute, Bijenička cesta 54, 10000 Zagreb, Croatia

[b]Department of Physics, Faculty of Science, University of Zagreb, Bijenička cesta 54,

10000 Zagreb, Croatia

ABSTRACT. A one-dimensional (1D) ladder-like coordination polymer $\{NH_4[\{Cu(bpy)\}_2(C_2O_4)Fe(C_2O_4)_3]\cdot H_2O\}_n$ (**1**; bpy = 2,2'-bipyridine) containing $[Cu(bpy)(\mu\text{-}C_2O_4)Cu(bpy)]^{2+}$ cationic units linked by oxalate groups of $[Fe(C_2O_4)_3]^{3-}$ building blocks was investigated as a new type of photoactive solid-state system. It exhibits a photocoloration effect when exposed to direct sunlight or UV/Vis irradiation. The photochromic properties and mechanism were studied by powder and single-crystal X-ray diffraction, UV/Vis diffuse reflectance, IR and EPR spectroscopy, magnetization and impedance measurements, and DFT calculations. The process of photochromism involves simultaneous intramolecular electron transfers from the oxalate ligand to Fe(III) and to $[Cu^{II}(bpy)(\mu\text{-}C_2O_4)Cu^{II}(bpy)]^{2+}$, leading to the reduction of the metal centres to the electronic states Fe(II) and Cu(I), accompanied by the release of gaseous CO_2.

INTRODUCTION

Stimulative and switchable materials exhibit two or more stable, observable or detectable properties in response to external stimuli (light, temperature, solvent molecules, pressure,...) at the micro- or nanoscale and have recently gained increasing attention for their potential applications in many fields. In general, there are three main types of stimuli: chemical, physical and biochemical. Chemical stimuli include pH, ionic solvents, chemical agents, etc.; physical stimuli are quite common, such as temperature, mechanical force, light, electric and magnetic fields; while biochemical stimuli include enzymes, ligands and so on.[1–6]

Photochromic materials are able to undergo reversible change in their molecular and electronic structure triggered by light irradiation. The reversible transformation of a chemical species between two forms, A and B, having different absorption spectra, is induced by the absorption of electromagnetic radiation. The thermodynamically stable form A is converted by irradiation to the less stable form B, which has different absorption spectra, and can be returned to form A either thermally or photochemically. The interconversion of two states is usually accompanied by the change of some physical properties, such as the refractive index, dielectric constant, electric conductivity, redox potential, structural transformation, solubility, viscosity, surface wettability, magnetism, luminescence, or a mechanical effect.[7–9]

Metal-organic coordination polymers have been recognized as a promising class of switchable materials because of their characteristic properties, excellent component and structure modulation ability due to the variety of inorganic nodes and flexibility of organic linkers. These materials are attractive because they allow convenient visual

monitoring of changes in specific property and therefore have potential applications in the fields such as optical switches, solar energy conversion, data storage or photomasks. There are several approaches that can be used to design photochromic metal-organic compounds. The most common method is the use of a photochromic linker that is able to undergo some structural change upon light irradiation. Alternatively, bipyridinium carboxylate linkers can be used to construct photochromic systems since they are able to generate viologen radicals when irradiated with light. Photochromic metal-organic coordination polymers without photochromic organic linkers can be engineered by making use of the photoinduced bistable systems based on different electron-transfer mechanisms. The photochromic mechanisms include metal-centered electron transition (MC), ligand-to-metal charge transfer (LMCT), metal-to-metal CT (MMCT), intraligand CT (ILCT), and ligand-to-ligand CT (LLCT). Photochromic metal-organic compounds with electron transfer are electronically labile, with their two or more electronic states energetically close to each other, leading to significant vibronic interactions and considerable sensitivity to external photo perturbations. The photoresponsive process depends on many factors such as the ability of electron-donors/acceptors to donate/accept electrons, the nature of packing, and weak interactions. For this reason, rational matching between units of electron donors and acceptors suitable for photoinduced electron transfer and subsequent radical generation is a very challenging task.[6,10–14]

One of the photoresponsive processes in metal-organic systems involves a LMCT reaction, in which an electron is transferred from the ligand to the metal centre, resulting in the formation of a radical ligand. A prototypical example of such complexes is the tris(oxalato)ferrate(III) complex, whose photoinduced LMCT reaction leads to the (photo)

generation of Fe(II) ions (both in solution and in the solid state) and to a subsequent reductive reaction *via* $CO_2^{\bullet-}$ radical anions.[15–19] From the applicative point of view photoreactive complexes sensitive to visible (Vis) and ultraviolet (UV) light could be of interest in environmental chemistry and photochemical laboratory applications in general (e.g. actinometry).[20]

In this context, we have studied compound $\{NH_4[\{Cu(bpy)\}_2(C_2O_4)Fe(C_2O_4)_3]\cdot H_2O\}_n$ (**1**; bpy = 2,2'-bipyridine) with $[Cu(bpy)(\mu\text{-}C_2O_4)Cu(bpy)]^{2+}$ cationic species units mutually connected through oxalate groups of $[Fe(C_2O_4)_3]^{3-}$ in a ladder-like one-dimensional (1D) coordination polymer as a new type of solid-state photoactive system.[21] This heterometallic compound exhibits significant photocoloration when exposed to direct sunlight or UV/Vis irradiation in the solid state. This observed effect was investigated by powder and single-crystal X-ray diffraction, UV/Vis diffuse reflectance, IR and EPR spectroscopy, magnetization measurements, impedance spectroscopy and DFT calculations. We have shown that the process of photocoloration involves simultaneous intramolecular electron transfers from the oxalate ligand to Fe(III) and to $[Cu^{II}(bpy)(\mu\text{-}C_2O_4)Cu^{II}(bpy)]^{2+}$, leading to reduction of the metal centres to Fe(II) and Cu(I) electronic states, accompanied by the release of gaseous CO_2.[15]

EXPERIMENTAL SECTION

Materials and Physical Measurements. All chemicals were purchased from commercial sources and used without further purification. The preparation method used for the synthesis of the ammonium salt of the tris(oxalato)ferrate(III), $(NH_4)_3[Fe(C_2O_4)_3]\cdot 3H_2O$, was derived from that of the potassium salt by replacing the potassium reactants with the

ammonium homologues.[22] The investigated compound $\{NH_4[\{Cu(bpy)\}_2(C_2O_4)Fe(C_2O_4)_3]\cdot H_2O\}_n$ (**1**) was prepared according to the procedure described in the literature.[21] Solid-state UV/Vis spectra were obtained at 20 °C using a Shimadzu UV-Vis-NIR spectrometer (model UV-3600) equipped with an integrating sphere. Barium sulphate was used as a reference. First, the initial sample was placed in the sample holder and measured, and then it was irradiated with a Xenon lamp (300 W) for 15 minutes and measured again. The infrared spectra were recorded in the 4000–350 cm^{-1} region with samples as KBr pellets, with a Bruker Alpha-T spectrometer.

Preparation of Irradiated Samples of Compound 1. The blue-green crystals or powder of compound **1** change colour to dark green (**1-irrad**) after irradiation under UV/Vis light. Irradiation was performed using an Asahi Spectra 300 W Xenon Light Source, model MAX-303, equipped with a UV-Vis mirror module (300–600 nm), a 422 nm long-pass filter and a light guide. The sample was placed 10 cm bellow the light source. After standing in the dark for 14 days, the sample **1-irrad** slowly changes colour back to greenish (**1-recov**). The effect of daylight on compound **1** was also studied (**1-irradD** *versus* **1-recovD**). The powder sample was left to stand on the bench for 5 days under laboratory conditions, during which it gradually turned dark green. For the IR measurements, the sample was irradiated with ten Luzchem LZC-UVA lamps (l_{exc} = 351 nm; P = 16 W).

Powder X-Ray Diffraction. The powder X-ray diffraction (PXRD) data at room temperature for samples **1** and **1-irrad** were collected in reflection mode with Cu Kα radiation on a Malvern Panalytical Empyrean diffractometer using a step size of 0.001° in the 2θ range between 5° and 50°.

Single-Crystal X-Ray Diffraction. Single-crystal measurements were performed on a Rigaku Oxford Diffraction Synergy S diffractometer with a HyPix hybrid pixel counting detector, using microfocus CuKα radiation.

EPR Study. Electron paramagnetic resonance (EPR) measurements were performed on powdered samples by an X-band EPR spectrometer (Bruker Elexsys 580 FT/CW) that was equipped with a standard Oxford Instruments model DTC2 temperature controller. The experiments were performed, using liquid nitrogen, in a temperature range 80–295 K. The microwave frequency was around 9.7 GHz, the magnetic field modulation amplitude was 0.5 mT and the modulation frequency was 100 kHz.

Magnetization Measurements. The static magnetization of **1** and **1-irrad** in the powder form was measured using a superconducting quantum interference device (SQUID) magnetometer. Measurements were performed at 300 K and field dependence of magnetization M(H) was measured several times to check reproducibility. Susceptibilities and effective magnetic moments were determined as the slopes of the linear M(H) dependences after correction for the contribution of the gelatine ampoule.

Electrical Study. The electrical conductivity of **1** and **1-irrad** in the form of a pressed pellet was measured by impedance spectroscopy (Novocontrol Alpha-N dielectric analyzer) in the frequency range of 0.01 Hz–1 MHz from 20 °C to 120 °C. For the electrical contacts, gold electrodes (3.8 mm in diameter) were sputtered on the opposite surfaces of the pellet. The impedance spectra were analysed by equivalent circuit modelling.

DFT Calculations. The density functional theory (DFT) calculations were performed using the Quantum ESPRESSO code v6.8.,[23,24] and the plane wave cutoff of 108 Ry was

used. The Brillouin zone was sampled with k-points of the density of at least 4 Å, using the so-called SSSP Efficiency pseudopotentials.[25] The PBE exchange-correlation functional[26] with +U correction[27] of 6 eV for Cu d orbitals and 2 eV for Fe d orbitals was used. The structure was relaxed until default criteria were met, i.e. the change in energy was less than 0.0001 Ry, and forces on all atoms were smaller than 0.001 Ry/a0. The unit cell was fixed to the experimental value.

RESULTS AND DISCUSSION

Crystal Structure of Compound 1 and Preparation of the Irradiated Compound 1. In this work, we have investigated the photoresponsive properties of a known 1D coordination polymer $\{NH_4[\{Cu(bpy)\}_2(C_2O_4)Fe(C_2O_4)_3]\cdot H_2O\}_n$ (**1**) crystalizing in a triclinic space group *P*-1. It was obtained using the building block approach, from the reaction of an aqueous solution of $[Fe(C_2O_4)_3]^{3-}$ and methanol solutions of Cu^{2+} and 2,2′-bipyridine by a layering technique, without the presence of daylight. Structural analysis revealed that this compound contains oxalate-bridged $[Cu(bpy)(\mu\text{-}C_2O_4)Cu(bpy)]^{2+}$ units linked by oxalate groups of the $[Fe(C_2O_4)_3]^{3-}$ anions to form the ladder-like 1D $[Cu^{II}Fe^{III}]$ chains along the *a* axis (Figure 1). Both copper atoms (Cu1 and Cu2) adopt 4 + 2 distorted octahedral coordination; however they are crystallographically and chemically inequivalent: the Cu1 atom is linked to the Fe1 atom by an -O–C–O- bridge, while the Cu2 atom forms bridge to the Fe1 atom only through an O atom of the oxalate molecule. The blue-green crystals of **1** are stable in the matrix in the dark for several months, and when dried from the matrix they can be stored in the refrigerator.[21]

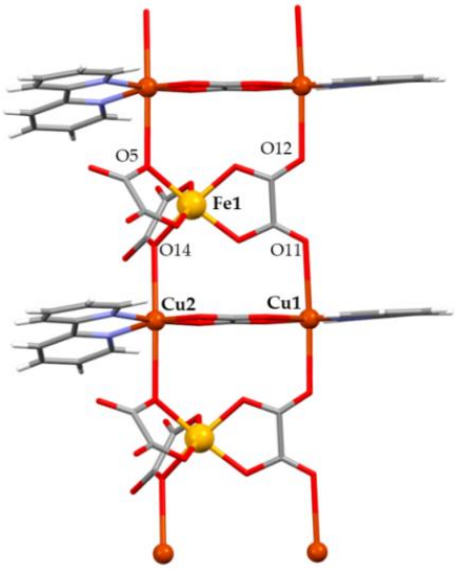

Figure 1. The ladder-like 1D chain motif in compound $\{NH_4[\{Cu(bpy)\}_2(C_2O_4)Fe(C_2O_4)_3]\cdot H_2O\}_n$ (**1**).

The crystals of compound **1** show eye-detectable colour changes when continuously exposed to UV/Vis light in air at room temperature (RT) (Figure 2a). Also, when continuously irradiated with UV/Vis light, the powder sample turns slightly dark in a matter of seconds (referred to below as **1-irrad**) (Figure 2b).

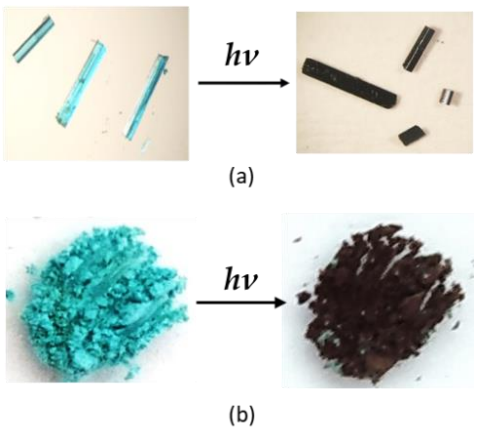

Figure 2. The photoinduced colour change of compound **1** (blue-green) to **1-irrad** (dark green) upon continuous irradiation with UV/Vis light of (a) single crystals for 15 minutes; (b) powder sample for 30 minutes.

It is noteworthy that blue-green compound **1** undergoes a photochromic transformation to a dark olive green (hereafter named as **1-irradD**) when exposed to daylight for 18 hours, after which no discernible colour change occurs (Figure 3). It should be noted that while many photochromic coordination polymers are known, those that respond to sunlight/daylight are relatively rare. In general, the use of sunlight for activation may facilitate the practical application of photochromic materials since sunlight is widely available.[28]

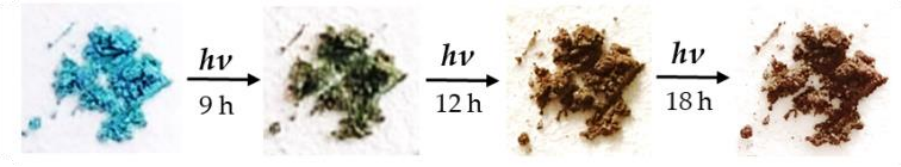

Figure 3. Photogenerated colour change of compound **1** after different daylight irradiation times.

The dark green **1-irrad** or **1-irradD** photoproduct is stable in air, and partially returns (visually) to its green colour, hereafter named as **1-recov** or **1-recovD**, after being stored in the dark under an ambient atmosphere for few months (Figure 4). The elevated temperature (70 or 130 °C) has no effect on the colour change of the crystals or powder of 1 in either direction. This slow, reversible transformation indicates that compound **1** has a photoinduced, long-lived, charge-separating state that has been shown to be important for the conversion from solar energy into chemical energy.[28] Many of the reported photochromic materials return to their initial colours within a few minutes.[29]

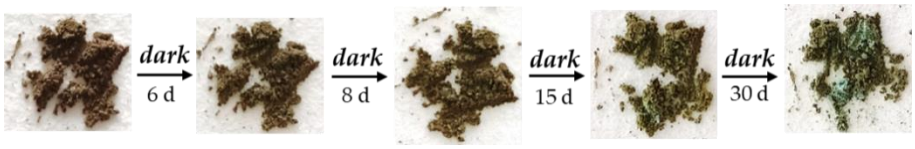

Figure 4. Daylight irradiated compound **1** after being stored in the dark for a different number of days (d).

The blue-green crystals of the isostructural compound $\{K[\{Cu(bpy)\}_2(C_2O_4)Fe(C_2O_4)_3]\cdot H_2O\}_n$ also undergo the same photochromic transformation as compound **1**,[21] whereas, as expected, the crystals of the isostructural compounds containing chromium(III) instead of iron(III), $\{A[\{Cu(bpy)\}_2(C_2O_4)Cr(C_2O_4)_3]\cdot H_2O\}_n$ ($A = K^+$ or NH_4^+), do not undergo.[30]

UV/Vis Solid State. The diffuse reflectance UV/Vis spectra before and after irradiation with UV/Vis light of **1** are shown in Figure 5. Before irradiation, the initial sample **1** (green line, Figure 5) shows overlapped absorption bands in the visible part of the spectrum which are related to: (*i*) d–$\sigma_{antibonding}$ transitions in the tetrahedrally elongated $[Cu(bpy)(C_2O_4)_2(\mu\text{-}C_2O_4)]$ octahedra (bands around 700 nm), and (*ii*) *d*–*d* transitions of

the high spin iron(III) atoms in distorted octahedral coordination with *O*-donors (bands around 410, 550 and 800 nm).[31]

After irradiation, the absorption intensity in the visible range increase, what is consistent with the blackening of the sample; a new band around 480 nm appears in the spectra, which is related to the ligand-to-metal charge transfer in the $Fe^{II}(C_2O_4)_3$ octahedra.[32] Moreover, in the irradiated sample, the bands corresponding to the transitions of Fe(III) octahedra vanish, and those related to the $[Cu(bpy)(C_2O_4)_2(\mu\text{-}C_2O_4)]$ octahedra decrease. This change in the optical properties triggered by UV/Vis light irradiation suggests the reduction of one Fe(III) to Fe(II), and one Cu(II) ion to Cu(I) enabled by the photoinduced oxidation of one oxalate ligand.[18]

When an irradiated compound is left in the dark, some of the Fe(II) ions are being oxidised back to Fe(III) in reaction with O_2 from the air. This process is very slow, and in the electronic spectra recorded after one month in the dark (1st recovery in Figure 6), the bands associated with Fe(II) ions decrease in intensity at 480 nm, and bands related to Fe(III) ions again appear at 410 and 550 nm. However, the initial spectrum (initial in Figure 6) is not completely recovered, indicating that oxidation occurs only on a fraction of the Fe(II) ions, as a result of the slow kinetics of the oxidation reaction with oxygen from the air at room temperature and pressure. In the following irradiation (2nd irradiation in Figure 6), the intensity of the band at 480 nm increases again, confirming that the recovered Fe(III) ions are again photoreduced to Fe(II). Hence, the colouration and bleaching process of the initial compound can be repeated at least 3 times by UV/Vis irradiation and standing in the dark; the intensity of the green and blackish colour decreases after each cycle.

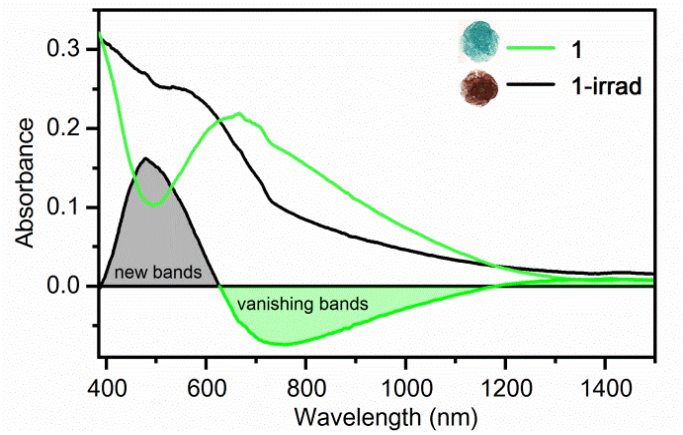

(a)

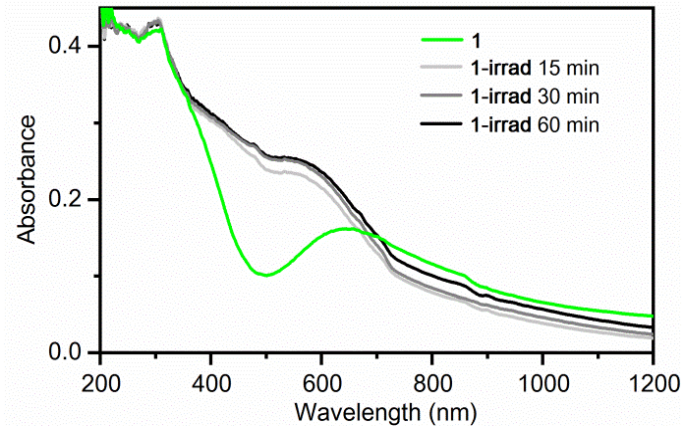

(b)

Figure 5. (a) Solid-state UV/Vis absorption spectra of **1** (green line) and **1-irrad** (black line), and the difference between the two spectra indicating changes in the electronic properties of **1** due to UV/Vis light irradiation; (b) Evolution of the photogenerated absorption during different irradiation times.

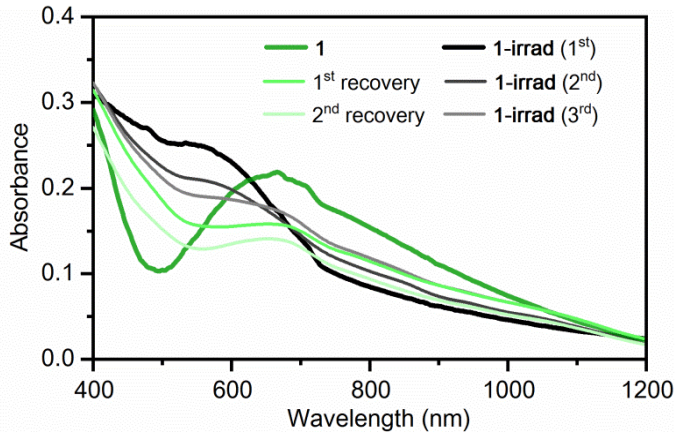

Figure 6. Solid-state UV/Vis absorption spectra of compound **1** before (green lines) and after UV/Vis irradiations (black lines). The initial compound underwent three repeated processes of the UV/Vis irradiation and standing in the dark.

IR Study. The IR spectra of compound $\{NH_4[\{Cu(bpy)\}_2(C_2O_4)Fe(C_2O_4)_3]\cdot H_2O\}_n$ pressed in a KBr pellet was recorded before and after irradiation with UV light (Figure 7) at different irradiation times (5 and 45 minutes). Before irradiation, the IR spectrum of **1** exhibits the absorption bands corresponding to the stretching vibrations of the uncoordinated {1709 and 1671 cm^{-1} [ν_{as}(CO)], 1385 cm^{-1} [ν_s(CO)], 794 cm^{-1} [δ(OCO)]} and coordinated {1645 cm^{-1} [ν_{as}(CO)], 1356 cm^{-1} [ν_s(CO)] and 781 cm^{-1} [δ(OCO)]} carbonyl of the bidentate-monodentate and bis(bidentate)/bidentate-bis(monodentate) oxalate ligands, respectively.[21] The most striking change in the irradiated sample is the appearance of very strong bands at 2355, 2341 and 666 cm^{-1} (Figure 7), which originate from the vibrations of carbon dioxide that is being released during the photodecomposition of oxalate and trapped in the KBr pellet during the experiment.[18,33,34] Upon irradiation, the intensity of the bands related to CO stretching vibrations gradually decreases with increasing irradiation time (Figure 7).

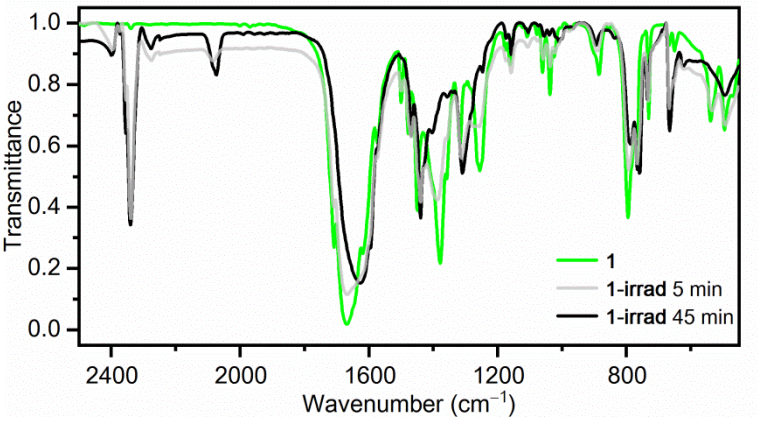

Figure 7. Irradiation-time dependence of the IR spectrum for compound **1**. Spectra were recorded at 298 K after 0, 5 and 45 minutes of irradiation with UV light.

These results also confirm a photodecomposition of the oxalate ligands of the tris(oxalato)ferrate(III) unit to the carbon dioxide. As expected, the intense bands of the oxalate groups coordinated to iron and exhibiting bidentate-monodentate mode change more rapidly than other oxalate bands (Figures 1 and 7). The band corresponding to the $\nu(Fe^{III}O)$ located at 538 cm^{-1} almost disappears after 45 minutes of irradiation; moreover, the intensity of the band at 494 cm^{-1} [δ(OCO)] decreases,[35] which is also broadened by the appearance of the $\nu(Fe^{II}O)$ band at 487 cm^{-1}.[36]

X-ray Diffraction Study. The powder X-ray diffraction (PXRD) verified that there was no obvious structural change before (**1**) and after irradiation (**1-irrad**) (Figure 8). This indicates that the photoresponsive behaviour is the result of a chemical charge transfer process rather than a structural transformation. As the photoinduced colour change is less intense after each irradiation (and recovery) cycle, in addition to diffraction lines corresponding to compound **1** broad humps can be also observed in PXRD. These humps are corresponding to the fraction of material in which the structure collapsed as a result of oxalate ligand consumption after each cycle of irradiation.

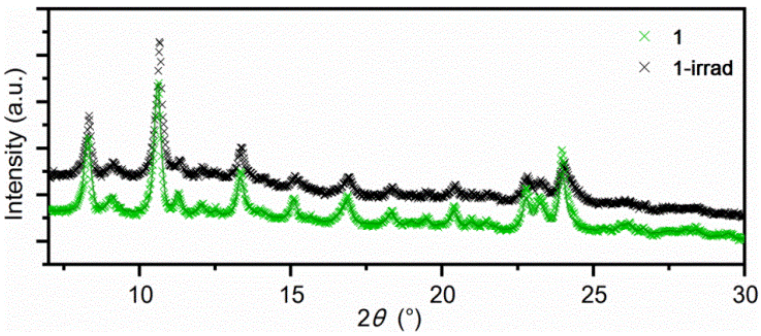

Figure 8. Powder XRD patterns of compound $\{NH_4[\{Cu(bpy)\}_2(C_2O_4)Fe(C_2O_4)_3]\cdot H_2O\}_n$ before (**1**) and after irradiation of 15 min (**1-irrad**).

In single-crystal experiment, a thin splinter of a crystal several μm thick was measured by X-ray diffraction before and after irradiation. Although the original green splinter (**1**) diffracted well (despite the small volume of the crystal), the darker **1-irrad** did not diffracted well. This led to the conclusion that the **1-irrad** phase is not crystalline enough for this method, due to the decomposition process of **1** by irradiation.

Magnetic Study. The magnetic properties of **1** have already been studied in detail, and from the temperature dependence of the magnetization it was concluded that the two Cu(II) ions with spin 1/2 are antiferromagnetically coupled into the spin singlet within the $[Cu(bpy)(\mu\text{-}C_2O_4)Cu(bpy)]^{2+}$ units, with relatively large super-exchange interaction across the oxalate bridge. The iron(III) ions have spin 5/2, and do not interact with copper(II) spins.[21] However, at room temperature the $\chi\cdot T$ product was slightly below the expected value for the independent spins of one iron(III) and two copper(II) ions per considered formula unit, due to the strong antiferromagnetic exchange between the copper(II) ions of −342 cm^{-1}, which somewhat reduces the overall magnetization.

In this work, the magnetization at room temperature was studied in terms of the field dependence of the molar magnetization $M_{mol}(H)$ for both **1** and **1-irrad**, the

measurements of which are shown in Figure 9. From the $M_{mol}(H)$ dependence for **1** at 300 K (dark green symbols), the slope is $(1.584\pm0.001)\cdot10^{-2}$ emu·mol^{-1}·Oe^{-1}, and after multiplication by the temperature 300 K, the product $\chi\cdot T$ is obtained to be (4.752±0.003) emu·K·mol^{-1}·Oe^{-1}. For completely independent spins, this product should be 5.24 emu·K·mol^{-1}·Oe^{-1} for one Fe(III) ion with spin 5/2 and two Cu(II) ions with spin 1/2, and the observed difference is comparable to the difference between the susceptibility of an antiferromagnetic dimer with super-exchange interaction of order 200–300 K and the susceptibility of two free copper(II) ions, which is in full agreement with previous study.[21] For all calculations the usual values of *g*-factors from the literature were used: 2.15 for copper and 2.0 for iron.[37] After irradiation, the sample was measured again in the magnetometer, and the $M_{mol}(H)$ dependence for **1-irrad** at 300 K (black symbols) significantly decreased compared with **1**. From the slope $(1.126\pm0.005)\cdot10^{-2}$ emu·mol^{-1}·Oe^{-1} multiplied by 300 K, the $\chi\cdot T$ product is (3.38±0.01) emu·K·mol^{-1}·Oe^{-1}. This value corresponds to one copper(II) ion with spin 1/2 and an iron(II) ion with spin 2, which would ideally give $3.435\cdot10^{-2}$ emu·mol^{-1}·Oe^{-1}, and this small difference could be ascribed to slightly different *g*-factors.

Therefore, the observed decrease in molar magnetization corresponds with a high probability to the conversion of Cu(II) into the diamagnetic Cu(I) in the cationic dimers, and of Fe(III) into Fe(II). According to the numbers, these changes take place in the vast majority of sample, which is possible due to the finely powdered microcrystals.

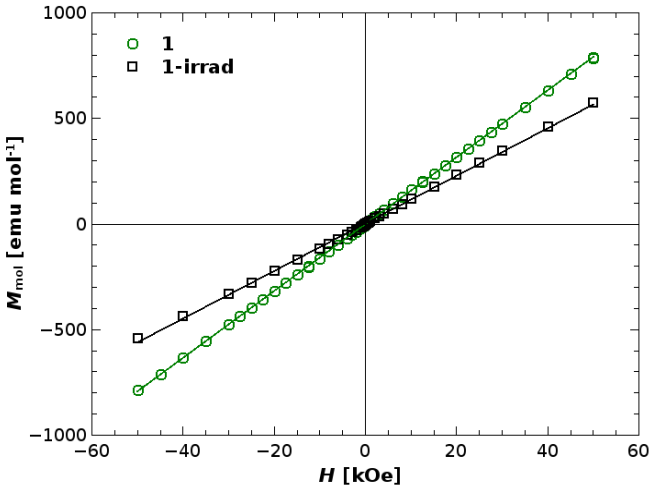

Figure 9. Field dependence of the molar magnetization of compound **1** measured at room temperature (300 K) before (dark green symbols and line) and after (black symbols and line) irradiation.

EPR Study. The light-induced colouration of **1** is accompanied also by an EPR study. Figure 10 shows the spectra of samples **1** and **1-irrad** (2 hours of irradiation) recorded at room (RT) and at low (LT, 80 K) temperature. The RT spectrum of **1** (Figure 10a) shows a signal from paramagnetic Fe(III) ions labelled by $g \approx 4.8$ (at line maximum position)[38] and one broad line around $g \approx 2.1$ that could be assigned to Cu(II) ions coupled through the oxalate bridge.[39] Besides these two lines, an additional line typical for paramagnetic (non-coupled) Cu(II), labelled by $g \approx 2.07$, could be seen.[40] After 2 hours of UV irradiation, Fe(III) line almost completely disappears. Additionally, the broad copper line around $g \approx 2.1$ also disappears. The irradiation-induced change in the EPR lines is more evident in the LT spectra, shown in Figure 10b, where the broad copper line is not observed due to stronger antiferromagnetic coupling between copper spins from the [Cu(bpy)(μ-C_2O_4)Cu(bpy)]$^{2+}$ units (see Magnetic study). As can be seen, the intensity of Fe(III) line decreases after irradiation. It should be stressed here that the mass of **1-irrad** sample was a few

times smaller compared to the mass of the pristine sample **1**, so a direct comparison of line intensities before and after the irradiation process is not possible. Additionally, it should be noted here, that Fe(II) ions are usually X-band EPR silent but their presence can be proved by bulk magnetization measurements or high-frequency EPR spectroscopy.

Electrical Study. The electrical conductivity of compound **1** before and after irradiation was measured by impedance spectroscopy. The complex impedance plot of **1** at 20 °C shows an arc at high values of impedance indicating very low electrical conductivity, whereas **1-irrad** exhibits a well-defined depressed semicircle at significantly lower values of impedance (see Figure 11). These experimental impedance data can be approximated by the equivalent circuit consisting of a parallel combination of resistor and constant phase element (CPE). The CPE is an empirical impedance function of the type Z*CPE= 1/[A(iω)α], where ω=2πf, f is the measuring frequency, i = (−1)1/2 is the imaginary unit, A is the constant, and α is a power law exponent with a value in the range of $0 < \alpha < 1$. For $\alpha = 1$, the CPE acts as an ideal capacitor, whereas for $\alpha = 0$, it is a resistor. The values of electrical resistance (R) at 20 °C of **1** and **1-irrad** obtained by the complex non-linear least squares fitting are given in the legends in Figure 11. From the value of electrical resistance (R) and electrode dimensions (A is the electrode area and d is the thickness of the sample), DC conductivity, σDC, was calculated according to relation: $\sigma_{DC} = d/(A \cdot R)$. The electrical conductivity of **1** at 20 °C is very low, $\sigma_{DC} = 8.8 \times 10^{-16}$ $(\Omega\ cm)^{-1}$, however it increases approximately four orders of magnitude upon irradiation [$\sigma_{DC} = 3.8 \times 10^{-12}$ $(\Omega\ cm)^{-1}$]. The observed increase in conductivity is in line with the structural and magnetic properties described in the previous sections, and can be related to the mixed oxidation states of iron and copper in an irradiated sample, which allow electron transfer to occur, hence increasing electrical conductivity.

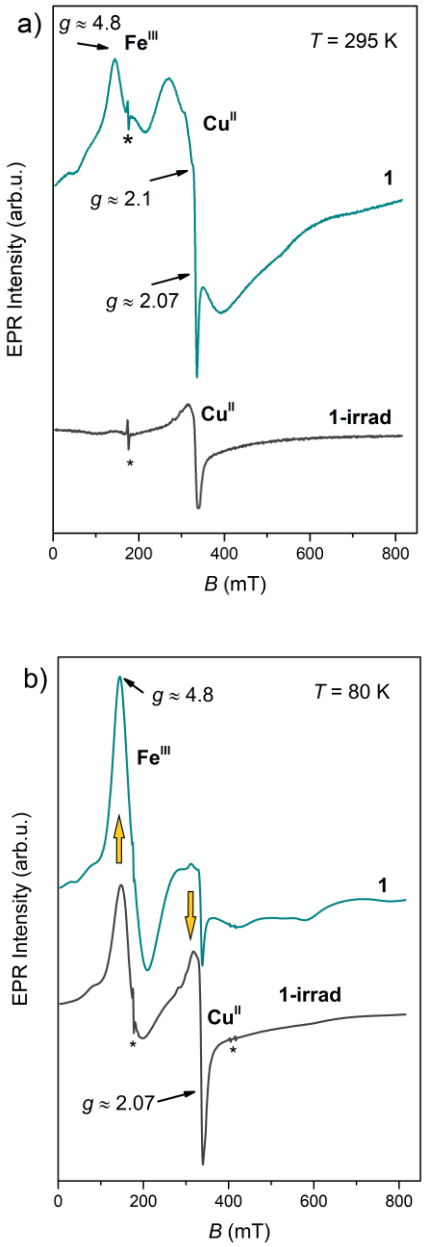

Figure 10. The EPR spectra of **1** and **1-irrad** recorded at (a) room temperature and (b) 80 K. Sharp lines labelled by asterisks are EPR cavity signal. The yellow arrows in (b) point to the direction of increasing EPR line intensities.

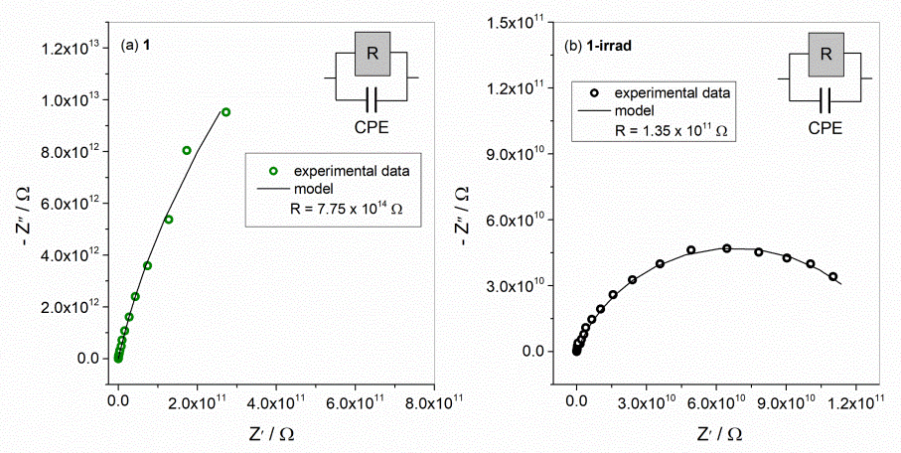

Figure 11. Complex impedance plots measured at 20 °C for (a) **1** and (b) **1-irrad** and their corresponding equivalent circuits.

DFT Calculations. The electronic structure of compound **1** was calculated with DFT. In agreement with other experiments, the obtained ground state consists of antiferromagnetically coupled Cu(II) ions and paramagnetic Fe(III) ions. Figure 12 shows the density of states projected on atomic orbitals per atomic type. Oxygen has the largest contribution to the top of the valence band, while the bottom of the conduction band is mostly made of Cu and Fe orbitals *d*. Upon irradiation, it is expected that electrons from the top of the valence band would fill the bottom of the conduction band, i.e. Cu and Fe orbitals *d*, which would explain the change from Cu(II) to Cu(I) and Fe(III) to Fe(II).

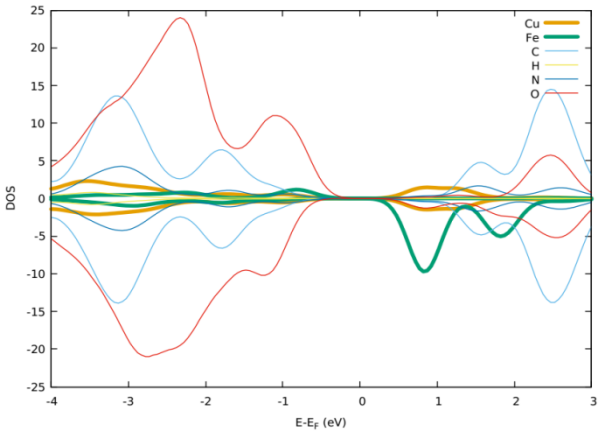

Figure 12. Projected electronic density of states of compound **1** obtained by DFT.

CONCLUSIONS

Compound **1** is a new photosensitive material that shows an intense coloration effect (from blue-green to black/dark green) in the solid state when irradiated with UV/Vis light or daylight. The effect is related to ligand-to-metal charge transfer, from the oxalate ligand to Fe(III) ions due to the partial photodecomposition of the oxalate ligand (photodissociation of the coordinated bond between Fe(III) and the oxygen atom) and reduction to Fe(II), together with the formation of a carbon dioxide radical ion ($CO_2^{\bullet-}$). Simultaneously, the radical ion most likely reacts with the cationic units $[\{Cu(bpy)\}_2(\mu\text{-}C_2O_4)]^{2+}$ forming reduced, diamagnetic Cu(I) ion and gaseous CO_2 is released. The other copper atom of the oxalate-bridged cationic moiety remains in the +2 oxidation state, as confirmed by magnetic research, implying that during the photocoloration process two electrons are released from the oxalate ligand and accepted by the metal atoms, followed by decomposition of the reactive oxalate.[18] This photochromic mechanism and the property changes caused by the irradiation were investigated, confirmed and explained by complementing different techniques and methods of characterization in the solid state before and after the irradiation of compound **1**: powder X-ray diffraction, diffuse reflectance UV/Vis, IR and EPR spectroscopy, magnetization and impedance measurements, and DFT calculations.

As functional molecular materials with stimulative and switchable properties are attracting interest from fundamental research to future applications, our further investigation would aim at the synthesis and characterization of novel complexes with the $[Fe(C_2O_4)_3]^{3-}$ core, leading to various photosensitive systems with tuneable properties based on electron transfer, as those of optical, magnetic and electrical in coordination polymer **1**.

ASSOCIATED CONTENT

Funding

This work has been funded and supported by the Croatian Science Foundation Project No. IP-2019-04-5742.

Notes

The authors declare no competing financial interest.

Acknowledgement

D. B. and D. P. acknowledge the support of project CeNIKS cofinanced by the Croatian Government and the European Union through the European Regional Development Fund – Competitiveness and Cohesion Operational Programme (Grant KK.01.1.1.02.0013). D. Ž. thanks HrZZ IP-2018-01-3168 project for financial support.

AUTHOR INFORMATION

Corresponding Author

***Dr. Marijana Jurić**
Ruđer Bošković Institure
Bijenička cesta 54
10000 Zagreb, Croatia

Phone: +385 1 4561189. Fax: +385 1 4680098.
E-mail: Marijana.Juric@irb.hr. (M.J.)

REFERENCES

(1) Ru, Y.; Shi, Z.; Zhang, J.; Wang, J.; Chen, B.; Huang, R.; Liu, G.; Yu, T. Recent progress of photochromic materials towards photocontrollable devices. *Mater. Chem. Front.* **2021**, *5*, 7737–7758.

(2) Rice, A. M.; Martin, C. R.; Galitskiy, V. A.; Berseneva, A. A.; Leith, G. A.; Shustova, N. B. Photophysics Modulation in Photoswitchable Metal−Organic Frameworks. *Chem. Rev.* **2020**, *120*, 8790−8813.

(3) Zhang, J.; Zou, Q.; Tian, H. Photochromic Materials: More Than Meets The Eye, *Adv. Mater.* **2013**, *25*, 378–399.

(4) Xiang, F.; Chen, S.; Yuan, Z.; Li, L.; Fan, Z.; Yao, Z.; Liu, C.; Xiang, S.; Zhang, Z. Switched Proton Conduction in Metal−Organic Frameworks. *JACS Au* **2022**, *2*, 1043−1053.

(5) Dunatov, M.; Puškarić, A.; Pavić, L.; Štefanić, Z.; Androš Dubraja, L. Electrically responsive structural transformations triggered by vapour and temperature in a series of pleochroic bis(oxalato)chromium(III) complex salts. *J. Mater. Chem. C* **2022**, *10*, 8024–8033.

(6) Li, H.-Y.; Xu, H.; Zang, S.-Q.; Mak, T. C. W.A viologen-functionalized chiral Eu-MOF as a platform for multifunctional switchable material. *Chem. Commun.* **2016**, *52*, 525–528.

(7) Han, S.-D.; Hu J.-X.; Wang, G.-M. Recent advances in crystalline hybrid photochromic materials driven by electron transfer. *Coord. Chem. Rev*. **2022**, *452*, 214304.

(8) Pardo, R.; Zayat, M.; Levy, D. Photochromic organic–inorganic hybrid materials. *Chem. Soc. Rev.* **2011**, *40*, 672–687.

(9) Dunatov, M.; Puškarić, A.; Androš Dubraja, L. Multi-stimuli responsive (l-tartrato)oxovanadium(v) complex salt with ferroelectric switching and thermistor properties. *J. Mater. Chem. C* **2023**, *11*, 2880–2888.

(10) Mehlana, G.; Bourne, S. A. Unravelling chromism in metal–organic frameworks. *CrystEngComm* **2017**, *19*, 4238–4259.

(11) Lustig, W. P.; Mukherjee, S.; Rudd, N. D.; Desai, A. V.; Li, J.; Ghosh, S. K. Metal–organic frameworks: functional luminescent and photonic materials for sensing applications. *Chem. Soc. Rev.* **2017**, *46*, 3242–3285.

(12) Haldar, R.; Heinke, L.; Wöll, C. Advanced Photoresponsive Materials Using the Metal–Organic Framework Approach. *Adv. Mater. 2020*, **32**, 1905227.

(13) Shen, J.-J.; Wang, F.; Yu, T.-L.; Zhang, F.-Q.; Tian, L.; Fu, Y.-L. Halogen-dependent photoinduced electron transfer and chromism of three protonated nicotinohydrazide halozincates. *Dalton Trans.* **2017**, *46*, 5414–5419.

(14) Rice, A. M.; Martin, C. R.; Galitskiy, V. A.; Berseneva, A. A.; Leith, G. A.; Shustova, N. B. Photophysics Modulation in Photoswitchable Metal–Organic Frameworks. *Chem. Rev.* **2020**, *120*, 8790−8813.

(15) Deguillaume, L.; Leriche, M.; Desboeufs, K.; Mailhot, G.; George, C.; Chaumerliac, N. Transition Metals in Atmospheric Liquid Phases: Sources, Reactivity, and Sensitive Parameters. *Chem. Rev*. **2005**, *105*, 3388–3431.

(16) Mangiante, D. M.; Schaller, R. D.; Zarzycki, P.; Banfield., J. F.; Gilbert, B. Mechanism of Ferric Oxalate Photolysis. *ACS Earth Space Chem.* **2017**, *1*, 270–276.

(17) Ogi, Y.; Obara, Y.; Katayama, T.; Suzuki, Y.-I.; Liu, S. Y.; Bartlett, N. C.-M.; Kurahashi, N.; Karashima, S.; Togashi, T.; Inubushi, Y.; Ogawa, K.; Owada, S.; Rubešová, M.; Yabashi, M.; Misawa, K.; Slavíček, P.; Suzuki, T. Ultraviolet photochemical reaction of $[Fe(III)(C_2O_4)_3]^{3-}$ in aqueous solutions studied by femtosecond time-resolved X-ray absorption spectroscopy using an X-ray free electron laser. *Struct. Dyn.* **2015**, *2*, 034901.

(18) Duan, Y.; Waerenborgh, J. C.; Clemente-Juan, J. M.; Giménez-Saiz, C.; Coronado, E. Light-induced decarboxylation in a photo-responsive iron-containing complex based on polyoxometalate and oxalato ligands. *Chem. Sci.* **2017**, *8*, 305–315.

(19) Muzioł, T. M.; Tereba, N.; Podgajny, R.; Kędziera D.; Wrzeszcz, G. Solvent-assisted structural conversion involving bimetallic complexes based on the tris(oxalato) ferrate(III) unit with the green → blue → red crystal color sequence. *Dalton Tran*s. **2019**, *48*, 11536–11546.

(20) Rabani, J.; Mamane, H.; Pousty, D.; Bolton, J. R. Practical Chemical Actinometry—A Review. Photochem. Photobiol. **2021**, *97*, 873–902.

(21) Kanižaj, L.; Androš Dubraja, L.; Torić, F.; Pajić, D.; Molčanov, K.; Wenger, E.; Jurić, M. Dimensionality controlled by light exposure: 1D versus 3D oxalate-bridged [CuFe] coordination polymers based on an $[Fe(C_2O_4)_3]^{3-}$ metallotecton. *Inorg. Chem. Front.* **2019**, *6*, 3327–3335.

(22) Inorganic Syntheses. ed. H. S. Booth, McGraw-Hill Book Company, INC., New York and London, 1939.

(23) Giannozzi, P.; Andreussi, O.; Brumme, T.; Bunau, O.; Buongiorno Nardelli, M.; Calandra, M.; Car, R.; Cavazzoni, C.; Ceresoli, D.; Cococcioni, M.; Colonna, N.; Carnimeo, I.; Dal Corso, A.; de Gironcoli, S.; Delugas, P.; DiStasio Jr, R. A.; Ferretti, A.; Floris, A.; Fratesi, G.; Fugallo, G.; Gebauer, R.; Gerstmann, U.; Giustino, F.; Gorni, T.; Jia, J.; Kawamura, M.; Ko, H.-Y.; Kokalj, A.; Küçükbenli, E.; Lazzeri, M.; Marsili, M.; Marzari, N.; Mauri, F.; Nguyen, N. L.; Nguyen, H.-V.; Otero-de-la-Roza, A.; Paulatto, L.; Poncé, S.; Rocca, D.; Sabatini, R.; Santra, B.; Schlipf, M.; Seitsonen, A. P.; Smogunov, A.; Timrov, I.; Thonhauser, T.; Umari, P.; Vast, N.; Wu, X.; Baroni, S. Advanced capabilities for materials modelling with Quantum ESPRESSO, *J. Phys.: Condens. Matter 2017*, **29**, 465901.

(24) Giannozzi, P.; Baroni, S.; Bonini, N.; Calandra, M.; Car, R.; Cavazzoni, C.; Ceresoli, D.; Chiarotti, G. L.; Cococcioni, M.; Dabo, I.; Dal Corso, A.; de Gironcoli, S.; Fabris, S.; Fratesi, G.; Gebauer, R.; Gerstmann, U.; Gougoussis, C.; Kokalj, A.; Lazzeri, M.; Martin-Samos, L.; Marzari, N.; Mauri, F.; Mazzarello, R.; Paolini, S.; Pasquarello, A.; Paulatto, L.; Sbraccia, C.; Scandolo, S.; Sclauzero, G.; Seitsonen, A. P.; Smogunov, A.; Umari, P.; Wentzcovitch, R. M. QUANTUM ESPRESSO: a modular and open-source software project for quantum simulations of materials. *J. Phys.: Condens. Matter* **2009**, *21*, 395502.

(25) Prandini, G.; Marrazzo, A.; Castelli, I. E.; Mounet, N.; Marzari, N. Precision and efficiency in solid-state pseudopotential calculations. *npj Comput. Mater.* **2018**, *4*, 72.

(26) Perdew, J. P.; Burkeand, K.; Ernzerhof, M. Generalized Gradient Approximation Made Simple. *Phys. Rev. Lett.* **1997**, *78*, 1396.

(27) Dudarev, S. L.; Botton, G. A.; Savrasov, S. Y.; Humphreys, C. J.; Sutton, A. P. Electron-energy-loss spectra and the structural stability of nickel oxide: An LSDA+U study. *Phys. Rev. B* **1998**, *57*, 1505.

(28) Kan, W.-Q.; Wen, S.-Z.; He, Y.-C.; Xu, C.-Y. Viologen-Based Photochromic Coordination Polymers for Inkless and Erasable Prints. *Inorg. Chem.* **2017**, *56*, 14926–14935.

(29) Li, P.-X.; Wang, M.-S.; Guo, G.-C. Two new coordination compounds with a photoactive pyridinium-based inner salt: influence of coordination on photochromism. *Cryst. Growth Des.* **2016**, *16*, 3709–3715.

(30) Kanižaj, L.; Molčanov, K.; Torić, F.; Pajić, D.; Lončarić, I.; Šantić, A.; Jurić, M. Ladder-like [CrCu] coordination polymers containing unique bridging modes of $[Cr(C_2O_4)_3]^{3-}$ and $Cr_2O_7^{2-}$. *Dalton Trans.* **2019**, *48*, 7891–7898.

(31) Solomon, E. I.; Lever, A. B. P. Inorganic Electronic Structure and Spectroscopy, John Wiley & Sons, Inc., Hoboken, New Jersey, 2006.

(32) Cococcioni, M.; de Gironcoli, S. Linear response approach to the calculation of the effective interaction parameters in the LDA+U method, *Phys. Rev. B* **2005**, *71*, 035105.

(33) Gerakines, P. A. Schutte, W. A. Greenberg J. M.; van Dishoeck, E. F. The infrared band strengths of H_2O, CO and CO_2 in laboratory simulations of astrophysical ice mixtures. *Astron. Astrophys.* **1995**, *296*, 810–818.

(34) Zhang, X.; Sander, S. P. Infrared Absorption Spectra of the CO_2/H_2O Complex in a Cryogenic Nitrogen Matrix—Detection of a New Bending Frequency, *J. Phys. Chem. A* **2011**, *115*, 9854–9860.

(35) Nakamoto, K. Infrared and Raman Spectra of Inorganic and Coordination Compounds. 6th ed., John Wiley, New York, 2009.

(36) Pegu, R.; Majumdar, K. J.; Talukdar, D. J.; Pratihar, S. Oxalate capped iron nanomaterial: from methylene blue degradation to bis(indolyl)methane synthesis. *RSC Adv.* **2014**, *4*, 33446–33456.

(37) Kahn, O. Molecular Magnetism. Wiley-VCH: New York, 1993.

(38) Bou-Abdallah, F.; Chasteen, N. D. Spin concentration measurements of high-spin ($g' = 4.3$) rhombic iron(III) ions in biological samples: theory and application. *J. Biol. Inorg. Chem.* **2008**, *13*, 15–24.

(39) Bencini, A.; Gatteschi, D. Electron paramagnetic resonance of exchange coupled systems. Springer, Berlin, 1990.

(40) Garribba, E.; Micera, G. The Determination of the Geometry of Cu(II) Complexes: An EPR Spectroscopy Experiment. *J. Chem. Educ.* **2006**, *83*, 1229–1232.

TABLE OF CONTENTS SYNOPSIS

1D ladder-like heterometallic compound obtained using $[Fe(C_2O_4)_3]^{3-}$, exhibits a photocoloration effect when exposed to direct sunlight or UV/Vis irradiation, which involves a simultaneous intramolecular electron transfers from the oxalate ligand confirmed by various techniques.